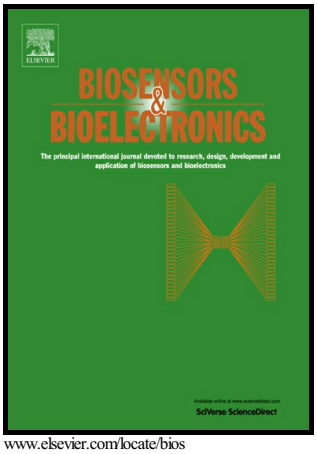

www.elsevier.com/locate/bios

A low-cost and miniaturized potentiostat for the monitoring of immunobiosensors by electrochemical impedance spectroscopy

Raquel Pruna, Francisco Palacio, Abdoullatif Baraket, Nadia Zine, Angelos Streklas, Joan Bausells, Abdelhamid Errachid, Manel López

PII: S0956-5663(17)30657-7
DOI: https://doi.org/10.1016/j.bios.2017.09.049
Reference: BIOS10023

To appear in: *Biosensors and Bioelectronic*

Received date: 26 July 2017
Revised date: 19 September 2017
Accepted date: 27 September 2017

Cite this article as: Raquel Pruna, Francisco Palacio, Abdoullatif Baraket, Nadia Zine, Angelos Streklas, Joan Bausells, Abdelhamid Errachid and Manel López, A low-cost and miniaturized potentiostat for the monitoring of immunobiosensors by electrochemical impedance spectroscopy, *Biosensors and Bioelectronic,* https://doi.org/10.1016/j.bios.2017.09.049

A low-cost and miniaturized potentiostat for the monitoring of immunobiosensors by electrochemical impedance spectroscopy

Raquel Pruna[a*], Francisco Palacio[a], Abdoullatif Baraket[b], Nadia Zine[b], Angelos Streklas[c], Joan Bausells[c], Abdelhamid Errachid[b], Manel López[a]

[a]Departament d'Enginyeries: Electrònica, Universitat de Barcelona, C/ Martí i Franquès 1, E-08028 Barcelona, Spain

[b]Université de Lyon 1, Institut des Sciences Analytiques, UMR 5280, CNRS, 5 rue de la Doua, F-69100 Villeurbanne, France
[c]Instituto de Microelectrónica de Barcelona, IMB-CNM (CSIC), Campus UAB, E-08193 Bellaterra, Spain

[*]Corresponding author. Tel.: +34 934 039 876. rpruna@el.ub.edu,

Abstract

Miniaturizing potentiostats, keeping their cost low and yet preserving full measurement characteristics (e.g. bandwidth, determination of capacitive/inductive contribution to sensor's impedance and parallel screening) is still an unresolved challenge in bioelectronics. In this work, the combination of simple analogue circuitry together with powerful microcontrollers and a digital filter implementation is presented as an alternative to complex and incomplete architectures reported in the literature. A low-cost acquisition electronic system fully integrated with a biosensors platform containing eight gold working microelectrodes and integrated reference and counter electrodes was developed and validated. The manufacturing cost of the prototype was kept below 300 USD. The performance of the proposed device was benchmarked against a commercial impedance analyzer through the electrochemical analysis of a highly sensitive biosensor for the detection of tumor necrosis factor α (TNF-α) within the randomly chosen range of 266 pg/mL to 666 ng/mL in physiological medium (PBS). A strong correlation between the outputs of both devices was found in a critical range of frequencies (1-10 Hz), and several TNF-α cytokine concentrations were properly discriminated. These results are very promising for the development of low-cost, portable and miniaturized electrochemical systems for point-of-care and environmental diagnosis.

Keywords: miniaturized potentiostat; cytokines; point-of-care; biosensors platform; electrochemical impedance spectroscopy; immunobiosensor.

1. Introduction

Heart failure (HF) is one of the fastest growing cardiovascular disorders (CVDs), since approximately 1 million new patients are diagnosed with this illness every year (Jessup and

Brozena, 2003; Lee et al., 2012). HF occurs when the heart cannot provide enough pump action to maintain an adequate blood flow, and it manifests in a number of symptoms such as shortness of breath, leg swelling and exercise intolerance (Gullestad et al., 2012; Nymo et al., 2014; Slaughter et al., 2010). To overcome the lack of donor organs, patients have been implanted with some bioelectronic devices such as pressure sensors and left ventricle assisted devices (LVADs). However, these clinical interventions result in increased risk of triggering upregulated inflammatory cytokine levels (e.g. Interleukin 1 (IL-1), IL-6, IL-8, IL-10, tumor necrosis factor α (TNF-α)) in blood and in saliva (Caruso et al., 2010; Kaptoge et al., 2014).

Immunoaffinity column assay, fluorimetric and enzyme-linked immunosorbent assay (ELISA) are amongst the traditional gold-standard techniques for the detection of CVD biomarkers (Caruso et al., 2012, 2010; Maurer et al., 2010; Navarri et al., 2015; Ooi et al., 2006; Soman et al., 2011; Watson et al., 2011). The two former techniques, although accurate and sensitive, require highly specialized personnel and huge sample volumes for analysis, since they are based on sophisticated instrumentation. On the other hand, ELISA is relatively affordable in terms of cost and expertise, but is still handicapped by the large amount of disposable material needed and for being time-consuming. Thus, there is an urgent need for easy-to-use, real-time and yet highly sensitive and selective diagnostic tools for early-stage detection of inflammatory biomarkers to enable rapid intervention and improve the patients' quality of life. In this light, biosensors present a low-cost, portable, reproducible, rapid, sensitive and label-free alternative (Alcacer et al., 2017; Baraket et al., 2016a, 2016b; Bellagambi et al., 2017; Benlarbi et al., 2012; Longo et al., 2016; Pui et al., 2011; Qureshi et al., 2012; Sánchez-Tirado et al., 2017), being electrochemical biosensors the most used among them (Kongsuphol et al., 2014). Several electrochemical biosensors have been developed for the monitoring of inflammatory cytokines. Electrochemical impedance spectroscopy (EIS) was used to detect IL-10 with a complementary metal oxide semiconductor (CMOS) based biosensor, achieving a limit of detection of 0.1 pg/mL (Lee et al., 2012). Similarly, a biocompatible and flexible biosensor based on gold microelectrodes was developed to detect TNF-α by EIS (Baraket et al., 2011). Also in the frame of TNF-α detection, Pui *et al.* developed an electrochemical impedance based biosensor achieving detection limits of 1-100 pg/mL in cell culture medium (Pui et al., 2013). A limit of detection of 10 pg/mL was achieved by Yin *et al.* by electrochemical monitoring of micropatterned aptamer-modified electrodes (Yin et al., 2011). Liu and coworkers reported electrochemical detection of TNF-α in whole human blood with an aptasensor, achieving a limit of detection of 10 ng/mL (Liu et al., 2013, 2012). On the other hand, it has been reported from the clinical point of view that plasma levels of TNF-α for HF patients in functional classes I to III is 1.95 ± 0.54, 2.63 ± 0.48 and 6.4 ± 1.9 pg/mL (Feldman et al., 2000; Torre-Amione et al., 1996), respectively. These are high cytokine levels compared to age-matched control subjects (0.75 ± 0.05 pg/mL). Careful interpretation of these results indicates that it is still difficult to meet detection limit requirements for TNF-α with current biosensors and measurement systems, and even more to discriminate between patient functional classes.

With all, most effort in the literature has been devoted to biosensor miniaturization, whereas commercial potentiostats are still large in most cases, and also expensive and time-consuming (Kaushik et al., 2014). Some trademarks have indeed commercialized portable versions of potentiostats (CH Instruments, Inc., 2017; Gamry Instruments, 2017; Hormiangz

LLC, 2014; Zensor Research & Development, 2016). Table 1 summarizes some technical specifications (focusing on impedance spectroscopy) of some of these portable and also of classic potentiostats, which can be directly benchmarked against the prototype presented in this work. Other characteristics such as geometry, weight and price are provided, as well as the number of channels available (at the indicated price) for real-time measurements. Overall, we are still far from meeting technical specifications such as frequency and voltage range presented by all commercial potentiostats, although our prototype can perform well in a variety of situations, as demonstrated hereinafter. Moreover, our prototype outperforms in terms of weight, number of channels (compared to portable, commercially-available potentiostats) and, most importantly, in terms of cost.

This illustrates the urgent need for low-cost miniaturized potentiostats that can be integrated into point-of-care (POC) diagnostic tools (Boyd and Woolley, 2016; Chin et al., 2012; Gomaa et al., 2016; Wang, 2006). In spite of the importance for this to be pursued, there are few proposals on low-cost miniaturized potentiostats in the literature, and they are still not easily embeddable into POC environments. In this context, Cruz and coworkers (Cruz et al., 2014) proposed a low-cost miniaturized potentiostat based on a LMP91000EVM commercial chip and a BeagleBone development board (Texas Instruments). The system was customized to perform cyclic voltammetry (CV) measurements for electrochemical immunosensing of cortisol, achieving a limit of detection of 1 pM. Here, the developed potentiostat was fully described, yet no impedance measurements were reported, which is indeed the issue at hand. In terms of portable impedance meters, Li *et al.* developed such an instrument in combination with a 3D-printed USB-compatible sensor chip for the detection of aflatoxins in rice. Here, the authors evaluated the performance of the developed device in relation to a Zahner commercial station (ZAHNER-elektrik GmbH & Co KG, Germany) (Li et al., 2016). A calibration curve showing the sensor impedance as a function of frequency was presented, indicating that their system cannot achieve frequencies below 100 Hz. This seriously compromises the versatility of the technique, hindering the use of the portable electrochemical station to measure other biosensors, as important features may be visible only at low frequencies. A more detailed system was presented by Yu *et al.* (Yu et al., 2016). They came up with an electronic architecture including open-loop rectifiers in order to determine absolute impedance values as well as two high speed complementary metal oxide semiconductor (CMOS) comparators and a two-input XOR gate followed by a low pass filter to measure impedance phases. However, only the absolute impedance *versus* frequency was shown, achieving good accuracy in their results. One could deduce that determining the impedance phase by hardware may not be the optimal approach. Another drawback of this system is that, again, frequencies below 100 Hz cannot be achieved, thus limiting its use in real-life biomedical environments. A very interesting approach was presented by Zhang *et al.* (Zhang et al., 2016). Here, the authors embedded a miniaturized commercial impedance analyzer (AD5933 from Analog Devices) into an integrated platform controlled by an Arduino UNO board. They also developed a smartphone application program and used a Bluetooth module to control the portable potentiostat. They tested the device with biological samples, and succeeded in detecting bovine serum albumin (BSA) at different concentrations. The main drawback was the limitation of the frequency range, which was 10 Hz – 10 kHz. This range was indeed wider than the range in previously cited works (Li et al., 2016; Yu et al., 2016), yet this may not be enough in some cases. As a matter of fact, many diffusion processes at the electrode-solution interface become important at low frequencies, i.e. below 10 Hz (Adachi et al., 2006; Bisquert et al., 2014,

1999; ter Heijne et al., 2015; Wang et al., 2005). Moreover, their system was customized to perform one measurement at a time, and at some point this should be overcome for the sake of immediacy and multiplexed monitoring of analytes.

In summary, the literature revised hitherto suggests that there are three main issues regarding the performance of low-cost portable potentiostats that have not been properly solved yet: (1) the expansion of the frequency range to low values, i.e. below 10 Hz (the reader should note from Table 1 that this is not an issue in the case of most commercially available miniaturized potentiostats, but they do not represent low-cost alternatives); (2) the determination of the capacitive/inductive contribution to the sensor complex impedance (magnitude and phase) and (3) the extension of the miniaturized electronic module to perform parallel measurements. In the present work we intend to individually tackle these issues. We developed a small and wearable potentiostat capable of measuring three-lead electrochemical biosensors, based on a well-described electronic circuit topology (Ahmadi et al., 2009, 2008). We designed some additional conditioning electronics to enable the measurement of eight parallel biosensors for redundant and/or multiplexed analyte detection, which is of crucial importance in some clinical and environmental scenarios (Barzen et al., 2002; Li and Macdonald, 2016; Petryayeva and Algar, 2014; Wang et al., 2015). Moreover, the developed potentiostat allows the user to choose between a pure DC voltage signal for the sensor excitation (thus eventually permitting the performance of cyclic voltammetry as well as amperometric measurements, amongst others) or a DC voltage bias plus a small AC signal at a desired frequency (to perform electrochemical impedance analysis). A graphical user interface (GUI) was also developed in MATLAB R2012a (The Mathworks, Inc.) to enable total control over the device, thus permitting the user to choose which of the eight biosensors to measure, or to measure all of them. The portable potentiostat was tested and validated for the detection of TNF-α cytokines at several concentrations in physiological medium, specifically within the range of 266 pg/mL to 666 ng/mL. The authors would like to remark that, as documented previously in this section, the latter is no clinically significant range, and it was chosen arbitrarily to illustrate the performance of the reported potentiostat. Future work will involve the detection of cytokines in real conditions, i.e. in blood and/or saliva in the case of TNF-α, and the characterization of biosensors in terms of linearity, limit of detection, sensitivity and specificity.

Table 1: Comparison of several commercial potentiostats with the presented prototype in terms of orientative cost, geometry and specifications. Information missing in empty fields was not possible to obtain.

	Price (USD)	**Freq. range (Hz)**	**V range (V)**	**Size W × D × H (cm^3)**	**Weight (g)**	**Channels**	**References**
ZENNIUM Electrochemical Workstation	-	10^{-5} – 4×10^{6}	-	36.4 × 16 × 37.6	11400	5	(ZAHNER-elektrik GmbH & Co KG, 2017)
Parstat MC	13 000	10^{-5} - 10^{6}	± 10	51.4 × 40.6 × 38.7	-	3	(Ametek Process & Analytical, 2015)
VMP3	100	10^{-5} -	± 10 /	49.5 × 46.5	20000	16	(Bio-Logic

	000	10^6	0-20	× 26			Science Instruments, 2016)
ACIP100	8 500	10^{-2} – 10^3	± 2	19.3 × 11.2 × 4.3	650	1	(Zensor Research & Development, 2016)
MicroAnalyzer 160C	3 200	10^{-2} - 10^5	± 2.4	10×6.4×2.4	150	1	(Hormiangz LLC, 2014)
CHI660E	13 000	10^{-5} - 10^6	± 10	36×24×12	5400	1	(CH Instruments, Inc., 2017)
Gamry 1010E	8 000	10^{-5} - 10^6	± 12	27×24×6	3000	1	(Gamry Instruments, 2017)
Our prototype	300	10^{-1} - 10^4	± 2.5	12×7×2	70	8	This work

2. Experimental: materials, methods and electronic design

2.1 Reagents

4-carboxymethyl aryl diazonium (CMA), sodium nitrite ($NaNO_2$), hydrochloric acid (HCl) 37 %, N-hydroxysuccinimide (NHS), N-(3-dimethylaminopropyl)-N′-ethyl-carbodiimide hydrochloride (EDC), potassium ferrocyanide (II), potassium ferricyanide (III) ($K_3[Fe(CN)_6]/K_4[Fe(CN)_6]$) and phosphate buffered saline (PBS) were purchased from Sigma–Aldrich, France. All immunoreagents, i.e. TNF-α cytokines and anti-TNF-α antibodies were purchased from R & D Systems, France.

2.2 Antibodies and cytokines preparation

Antibodies and cytokines were diluted in PBS buffer, aliquoted, and stored at -20 °C following the protocol of the supplier. The TNF-α cytokines were aliquoted before EIS measurements at three arbitrary concentrations: 266 pg/mL, 13 ng/mL and 666 ng/mL, and stored at 4 °C. The anti-TNF-α antibody solution was aliquoted at 2.5 µg/mL in PBS.

2.3 Miniaturizing the biosensor. Gold WEs chemical modification

The fabrication and characterization of the miniaturized biosensor platform has been previously described (Baraket et al., 2016a). Prior to CMA electroaddressing, the gold working microelectrodes (WEs) surfaces were cleaned with ethanol in an ultrasonic bath for 10 minutes and dried under a gentle stream of nitrogen. The device was then placed under UV/ozone for 20 minutes in order to remove all organic contaminants. In parallel, CMA (5 mM) was diazotated in an aqueous solution of HCl (20 mM) and $NaNO_2$ (20 mM) for 10 minutes at 4 °C. Then, four repetitive CV cycles between 0 V and -1 V were applied to the gold WEs, with a scan rate of 100 mV/s. Afterwards, the anti-TNF-α monoclonal antibodies were covalently attached to the CMA-coated WEs by EDC/NHS (0.1 M) crosslinking both at 0.1 M following a protocol available in the literature (Bellagambi et al., 2017). All eight gold WEs were functionalized and measured after the same protocol.

2.4 Miniaturizing the potentiostat. Design and development of the electronic system

The electronic board that was designed and customized as a miniaturized potentiostat is hereby described in two well-distinguishable parts: the digital and the analogue stages (Fig. 1a). The power supply stage is described in an additional section for the sake of legibility. The digital stage includes two microcontrollers (µCs) for waveform generation, response acquisition, optional further *in situ* signal post-processing and serial communication with a computer and optionally with other modules. On the other hand, the analogue part includes an electronic circuit topology based on operational amplifiers (OpAmps) and feedback loops for measuring three-lead electrochemical biosensors. A GUI was developed in MATLAB to help the user set measurement parameters such as frequency and voltage amplitude, and for post-processing purposes. The GUI main window is shown in Fig. 1b and further described in subsection 2.4.2.

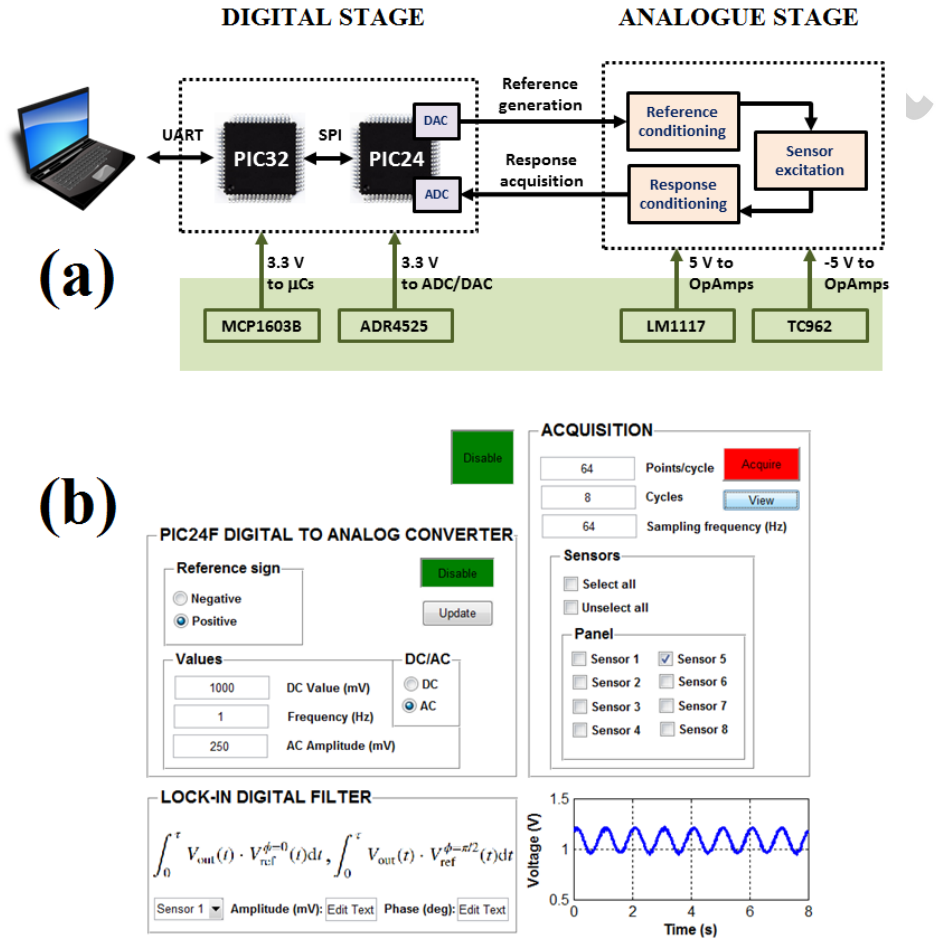

Fig. 1: (a) High level representation of the portable potentiostatic device, showing the interaction between the digital and analogue stages. The green region comprises the electronic elements responsible for power supply. (b) The graphical user interface and post-processing algorithms were developed in MATLAB. Here, measurement parameters such as frequency, DC polarization and small AC amplitude can be introduced in the GUI main window. This interface also allows for determination of positive/negative reference sign, and the user may choose between sensors 1-8 to measure the corresponding electrochemical impedance.

2.4.1 Power supply

A power supply stage is necessary to guarantee the correct operation of each active component in the board (green region in Fig. 1a). Four low-power integrated chips were required in the present approach. Regarding the digital stage, the MCP1603B (Microchip) is a 2.0 MHz synchronous buck regulator that supplies both µCs with 3.3 V. Although the analogue-to-digital and digital to analogue converters (ADC/DAC) are embedded in the µCs, they require additional power supply in order to guarantee a stable voltage reference. This was provided by the low-noise and low-power ADR4525 from Analog Devices. As for the analogue part of the potentiostatic system, the LM1117 (Texas Instruments) linear regulator and the TC962 (Microchip) high voltage DC-to-DC converter were used to have a bipolar (5 V and -5 V) supply to the OpAmps.

2.4.2 Digital stage

In this section we will focus on the description of the digital part of the potentiostatic system, which comprises the intercommunication of two µCs and the computer interface. The PIC32MX795F512L (Microchip), PIC32 hereafter, is a 32-bit, 80 MHz, 1.56 DMIPS/MHz, M4K core with a five stage pipeline and Harvard architecture microcontroller that was given the role of central control unit in the potentiostat. It was programmed to interface a computer via its UART/USB peripheral. Simultaneously, the PIC32 was also programmed to establish serial communication with an additional PIC24FJ128GC010 (Microchip), PIC24, microcontroller based on a serial peripheral interface (SPI) protocol. A quick look at Fig. 1a reveals the role of each µC in the system. In this respect, the PIC24 µC is responsible for waveform generation (sensor excitation) and acquisition of sensor's response for subsequent transmission to the PIC32. To do so, it includes a 10-bit DAC and a 16-bit ADC, respectively. This PIC24's 16-bit ADC is optimal for acquisition in the present application compared to the PIC32, whose 10-bit ADC could impede meeting the required standards of resolution and thus precision. In addition, the PIC32 has no DAC, and thus an external waveform generator would have been required. On the other hand, the PIC32 allows for better processing performance and data storage due to its 32-bit core. *In situ* signal post-processing will be implemented in the future, and if only the PIC24 had been included in the digital architecture, the need for further storage capacity would have arisen. Furthermore, the use of two separate microcontrollers for signal processing and data logging will eventually enable simultaneous measurement and data analysis with one device, which will speed up the monitoring process. Appendix A in the supplementary information includes a flowchart to illustrate the firmware implementation in both microcontrollers.

In parallel, a GUI was developed in MATLAB (1) to set voltage reference parameters and (2) for post-processing of the acquired sensor response. The software implementation of the GUI and processing algorithms is also described in Appendix A. Briefly, the first panel in the GUI (Fig. 1b) allows for selection between positive or negative voltage reference signals. Regarding the desired electrochemical analysis, a pure DC voltage or a DC plus small AC signal is required. DC offset, AC amplitude and frequency need to be input by the user. In the acquisition panel, WEs 1-8 may be selected for response acquisition and plotting. Signal post-processing was done in the lock-in digital filter panel, where the deduced amplitude and phase were shown for the chosen WEs. As an alternative approach, the PIC32 could be programmed to autonomously generate the excitation signal and also to perform the necessary post-processing steps in case no computer was available. This may be useful in portable and autonomous lab-on-a-chip configurations, where the signal processing would be done *in situ* and displayed on the lab-on-a-chip device. However, this

approach has a strong disadvantage: the reference voltage signal and frequency limits should be fixed *a priori*, and changing them would imply the need for reprogramming the board.

2.4.3 Analogue stage

First task in the analogue stage is to implement proper "Reference signal conditioning" (Fig. 2) electronics. As the DAC in the PIC24 µC works between 0 and 3.3 V, the reference excitation signal is always generated in the positive voltage domain. Nevertheless, regarding the intrinsic nature of the biosensor under study, the user may need a negative voltage. To solve this, specific analogue circuitry was implemented in the electronic board. A switch allows the selection between either an inverter circuitry of gain 1 to create a negative reference from the positive one or a follower circuitry to maintain the positive reference. As already explained in the previous section, the user just needs to select the "negative" option in the DAC reference sign panel in the GUI (Fig. 1b). In the analogue circuitry of the "Reference signal conditioning" stage, 1 nF decoupling capacitances were added to avoid interferences. Moreover, an additional switch was added in order to choose between a DC offset plus a small AC signal or a pure DC excitation signal. This once again is up to the user and the electrochemical measurement required to be performed on the biosensor, and needs to be indicated in the GUI. For instance, amperometry or cyclic voltammetry (CV) require DC signals, whereas for electrochemical impedance spectroscopy (EIS) analysis, small AC signals need to be applied to the sensor. As in typical three-lead electrochemical cell configurations, the reference voltage is applied to the biosensor between the reference (RE) and the working electrode (WE). In order to maintain this voltage constant, an electrical current flows between the counter electrode (CE) and the WE. This is described in the "Sensor excitation" stage in Fig. 2. Furthermore, a "Sensor response acquisition" stage is needed in order to translate the aforementioned current flowing through the biosensor into a measurable voltage. For this purpose, a transimpedance amplifier (TIA) configuration with a feedback resistor R_f was used. Finally, and since the latter is an inverter configuration, the final "Sensor response conditioning" stage consists of a unity gain inverter configuration to obtain a positive voltage signal that can be digitalized by the ADC in the PIC24 microcontroller. Fig. 3 shows the printed circuit board (PCB) of the miniaturized potentiostat connected to the biosensor platform. It is worth mentioning that stages 3 to 5 were implemented eight times in the board, since the biosensor array included eight integrated WEs. This was useful for performing eight measurements in parallel either for detecting different analytes or to study the repeatability of one single measurement.

Throughout the analogue stage, several OpAmps were employed. These can be sorted into two groups, regarding the technical specifications required for each of them. The OpAmp used in the "Sensor excitation" stage (labelled as OA2 in Fig. 2) was the LPC662 (Texas Instruments). The only requirement at this stage was that the OpAmp had high enough input impedance (> 1 TΩ in the present case, which is achieved by an ultra-low input bias current of 2 fA), so that it could measure sensors with arbitrarily high impedance; otherwise, it would modify the measured sensor impedance. It should be noticed that the rest of OpAmps in the other stages act as voltage followers or as TIAs, and thus they require maximum precision in order to guarantee the output at the OpAmps. These were labelled as OA1 in Fig. 2, and the AD8672 from Analog Devices was chosen in this case. Here, the OpAmp's maximum precision is achieved due to a low input impedance that prevents any external undesired frequency to be coupled to the signal.

It is worth mentioning that the response signal may not be clean enough to properly deduce the sensor's impedance features. Possible noise sources may arise from (1) the biosensor's intrinsic nature, (2) undesired instabilities of certain electronic components in the potentiostat at some frequencies, (3) the coupling of the network's electrical noise (50/60 Hz and corresponding harmonics), (4) instabilities in the acquisition stage, etc. Indeed, oscillations due to instabilities of the TIAs in the circuitry at certain frequencies were detected due to the capacitive nature of the systems to be measured. Open-loop gain of operational amplifier-based circuitry with feedback such as the one we are dealing with is frequency-dependent, and from Barkhausen stability criterion, oscillations appear if the TIA circuit does not have sufficient phase margin (Bhat, 2012). The latter may be achieved by adding a bypass capacitor C_f (Fig. 2) in parallel with the feedback resistance, R_f. The values of R_f and C_f need to be regulated regarding the effective impedance of the sensor. Here, values of 150 kΩ and 1 µF were enough to cover the whole range of measured impedances.

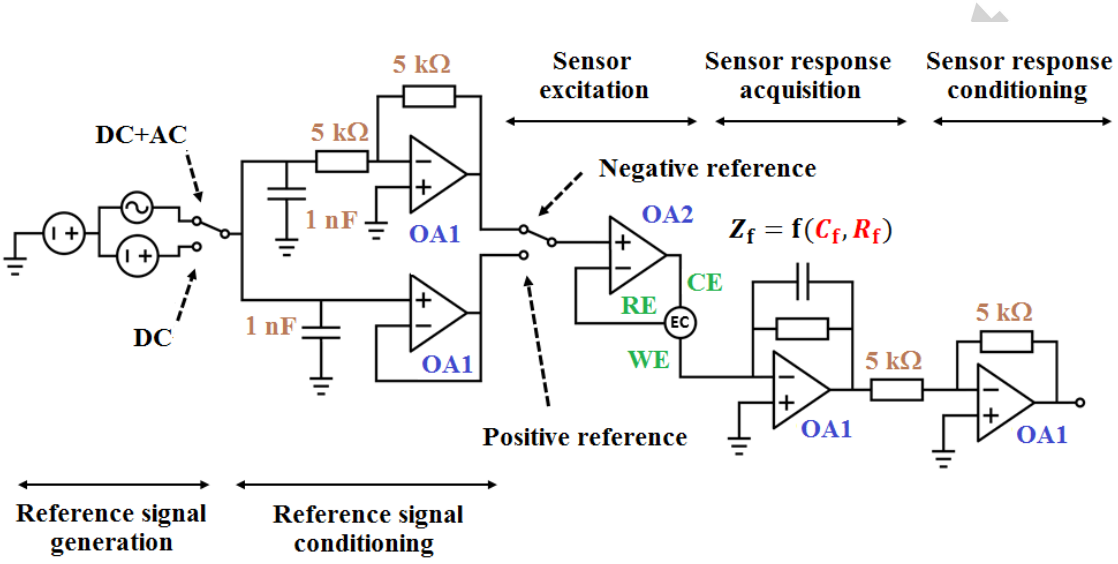

Fig. 2: Schematic of the electronics behind the portable potentiostat, including five main different stages: (1) the "reference signal generation", to choose between pure DC signal or DC bias plus small AC voltage; (2) the "reference signal conditioning" to select the sign of the voltage signal excitation; (3) the "sensor excitation" stage including a three-lead connection to an electrochemical cell (EC); (4) the inverter "sensor response acquisition" stage to transform the sensor response current to a measurable voltage, and finally, (5) the "sensor response conditioning" as a signal adaptation stage before ADC acquisition. OpAmps labelled as OA1 correspond to AD8672, whereas OA2 corresponds to LPC662. The feedback impedance Z_f can be calculated as a function of adjustable C_f and R_f.

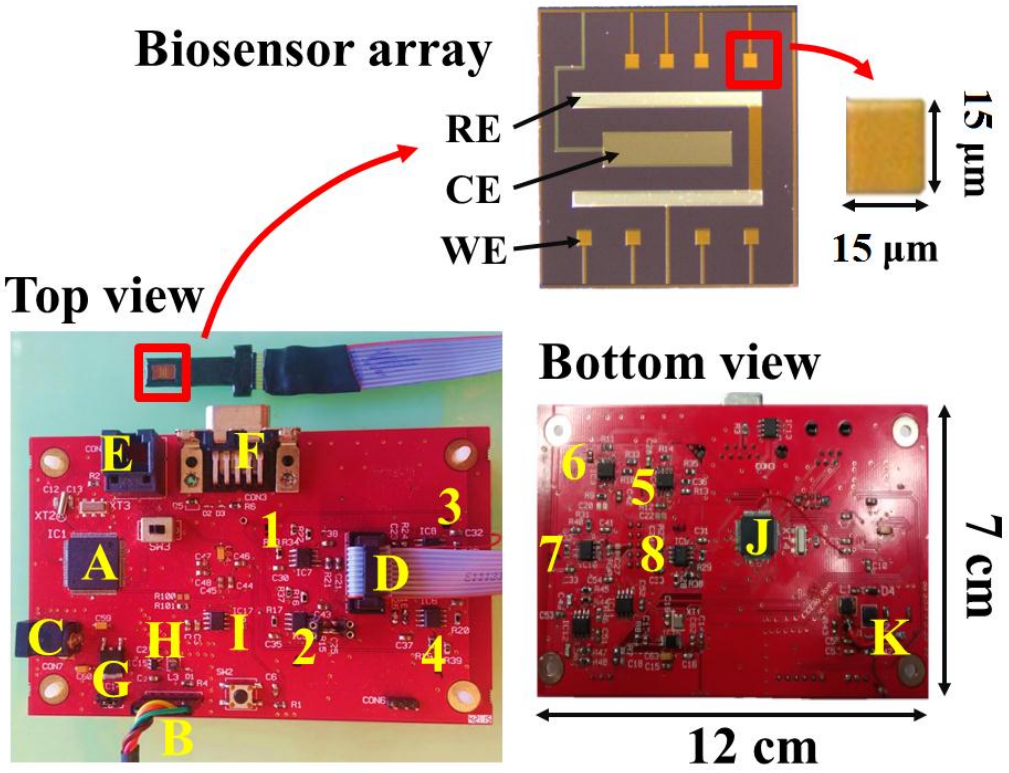

Fig. 3: Manufacturing details of the PCB and the biosensor array. Several electronic components are indicated in the top and bottom views of the PCB. The potentiostatic circuits for the different channels are labelled as 1-4 (top view) and 5-8 (bottom view). Regarding the rest of the elements, A) is the PIC32 microcontroller; B) is the UART connector for PC communication; C) is the external power supply; D) is the 10-pin connector for the biosensor array; E) is the RJ-11 connector to program the microcontrollers; F) is the data bus; G) is the LM1117 voltage regulator; H) is the MCP1603B voltage regulator; I) is the ADR4525 stable voltage reference; J) is the PIC24 microcontroller and K) is the TC962 voltage regulator.

2.4.4 Signal processing and extraction of parameters

The digital implementation of a lock-in amplifier was used to extract the sensor response signal within a known carrier wave, the frequency of which was fixed by the excitation signal. Once the sensor response is known, i.e. the amplitude and phase shift of the acquired periodic signal, the determination of the sensor impedance just involves an $R_f|C_f$ feedback gain, as explained in section 2.4.3. From careful circuit analysis of Fig. 2, the following expression for the sensor impedance as a function of known parameters can be deduced:

$$Z_s = \frac{V_{ref}(\omega_r t + \varphi_r)}{V_{out}(\omega_r t + \varphi_s)} Z_f, \quad (1)$$

where Z_f is the complex feedback impedance, $V_{ref}(\omega_r t + \varphi_r)$ is the voltage reference signal and $V_{out}(\omega_r t + \varphi_s)$ is the response of the sensor to the reference excitation. Note that the frequency of the sensor response should be the same as the reference signal's, with an additional phase and gain accounting for the intrinsic nature of the sensor. However, due to interferences and additional noise, extra frequencies mask the desired and pure response. Equation 1 is true under the assumption that the equivalent solution resistance is negligible

compared to the equivalent polarization resistance of the biosensor. The lock-in amplifier method consists in extracting the characteristic parameters (sensor response amplitude, V_s, and phase shift with respect to reference signal, $\Delta\varphi = \varphi_s - \varphi_r$) of the response to a single-frequency well-defined excitation signal (reference) in an extremely noisy environment (Burdett, 2005; Scofield, 1994). The lock-in filter is mathematically described in the Appendix B supplementary file.

2.5 System validation and performance

Having implemented the basic potentiostat as well as the necessary compensation circuitry, we proceeded to the calibration of the device. The validation process was performed with known SMD electrical components simulating Randles equivalent circuits (Lasia, 2002; Randles, 1947). A system composed of 1.5 kΩ in series with the parallel of 1 nF and 150 kΩ was used as a proof of concept (equivalent circuit shown as inset in Fig. 4). Nine frequencies were taken between 100 mHz and 10 kHz, and the impedance magnitudes as well as phases were deduced and compared with the theoretical values from impedance analysis, as shown in Fig. 4. A sinusoidal AC signal of 500 mV peak-to-peak amplitude with a DC offset of 1 V was used for the calibration of the device. The results shown in Fig. 4 demonstrate the applicability of the developed potentiostat in terms of frequency range and also the power of the lock-in digital filter to discriminate the impedance magnitude and phase.

The integrated biosensor array was first electrochemically characterized with a commercial VMP3 multichannel potentiostat (Biologic-EC-Lab, France). All the experiments were carried out at room temperature in an aqueous solution of 5 mM $K_3[Fe(CN)_6]/K_4[Fe(CN)_6]$ in PBS buffer at pH 7.4. CV was used to characterize the bare gold WEs, to electroaddress the CMA coatings and finally to characterize the CMA-modified WEs. EIS with commercial potentiostat was performed onto bare gold WEs and after each step of functionalization: after CMA deposition, after antibody modification and at three cytokine concentrations. After each EIS spectrum performed with the commercial potentiostat, the data were fitted by EC-Lab software. Extraction of EIS parameters gave enough information to optimize the feedback elements in the portable miniaturized potentiostat.

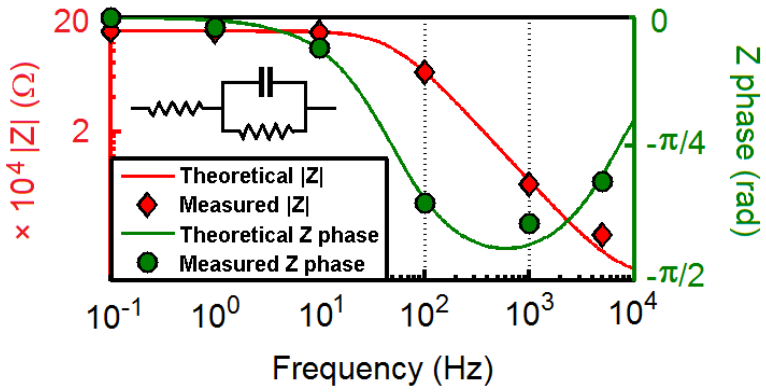

Fig. 4: Bode plot of the equivalent circuit shown in the inset as a proof of concept, showing both theoretical and measured impedance (magnitude in Ω and phase in radians), from 100 mHz to 10 kHz.

3. Results and discussion

3.1 Diazonium-antibody immobilization onto gold WEs

Fig. 5a shows the voltammogram corresponding to the electroaddressing process of CMA deposition onto gold WEs. It consists of an initial broad and irreversible cycle with a peak potential at -0.8 V, which corresponds to the reduction of diazotated CMA onto the bare gold WEs surface. The immobilization of this salt was also confirmed by a difference in the shape of CV before and after gold modification, as can be observed in Fig. 5b. A huge decrease in peak-to-peak intensity corresponding to reduction/oxidation of $K_3[Fe(CN)_6]/K_4[Fe(CN)_6]$ on the electrode surface is observed as a result of a large passivation area in the microelectrodes.

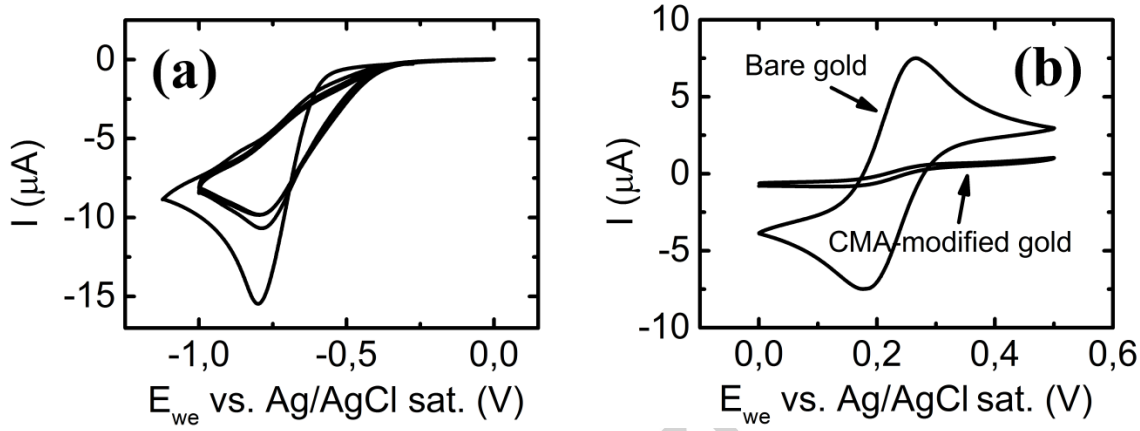

Fig. 5: Cyclic voltammetry showing (a) CMA deposition onto gold WEs. Four repetitive scans were performed at 100 mV/s from 0 V to -1 V *vs*. integrated Ag/AgCl. (b) Difference in voltammogram shapes between bare gold and CMA-coated gold WEs. These were performed at a scan rate of 50 mV/s from 0 V to 0.5 V *vs*. integrated Ag/AgCl reference electrode.

3.2 Cytokine detection by EIS with commercial potentiostat

EIS was performed with the commercial potentiostat to characterize each functionalization step. The measurements were taken in PBS buffer solution of 5 mM $K_3[Fe(CN)_6]/K_4[Fe(CN)_6]$ at pH 7.4 for all WEs. Fig. 6a shows Nyquist plots of all steps performed on a representative WE. First semicircle corresponds to CMA-coated gold WE, which is considerably bigger than the bare gold WE Nyquist plot, shown as inset. The second semicircle corresponds to the immobilized anti-TNF-α antibodies. Prior to cytokines incubation, the electrodes were rinsed abundantly with PBS to remove possible remaining electrolyte solution from the sensitive layer. The biosensor was then immediately immersed in a 266 pg/mL solution of TNF-α cytokines for 30 minutes incubation at 4 °C. It is of crucial importance to perform this step as carefully and fast as possible, in order to prevent denaturation of the immobilized antibodies. Afterwards, the unbounded cytokines were removed by abundant rinsing with PBS, and EIS was performed. The corresponding Nyquist plot proves for antigen-antibody recognition. These steps were repeated for subsequent increasing cytokines concentration (13 ng/mL and 666 ng/mL), providing the corresponding increase in electrochemical impedance, as shown in Fig. 6a.

3.3 Cytokine detection by EIS with miniaturized potentiostat

From the Nyquist plots shown in Fig.6a it can be deduced that the maximum impedance variation between subsequent steps was measured in the frequency range of 1-10 Hz. Thus, the portable electronic board was programmed to perform impedance measurements in such frequency range. The measurements were taken immediately after those with the commercial device. Results are shown as a Bode plot in Fig. 6b. The relation between the absolute impedance at 1 Hz measured by the portable and the commercial potentiostats is shown as a linear calibration plot in Fig. 6c.

We demonstrated that our device can perform electrochemical impedance spectroscopy at frequencies as low as 100 mHz, and also that the lock-in digital filter is useful for discrimination of impedance amplitude and phase, as shown in Fig. 4. In the present case, frequencies above 10 kHz are tricky, especially when the sensor impedance achieves very low values. In such cases, the device response is saturated, for the system total gain is $\frac{Z_f}{Z_s}$. A solution to this could be lowering $|Z_f|$, at the risk of a possible noise coupling at low frequencies. Thus, the most efficient solution would be the implementation of a digital feedback resistor selector, e.g. a multiplexer. This will be considered in future work. Moreover, the implementation of fitting functionality in the MATLAB based GUI will be also addressed in the future, in pursuit of self-contained software to account for important electrochemical parameters measured by this compact and total autonomous miniaturized impedance analyser.

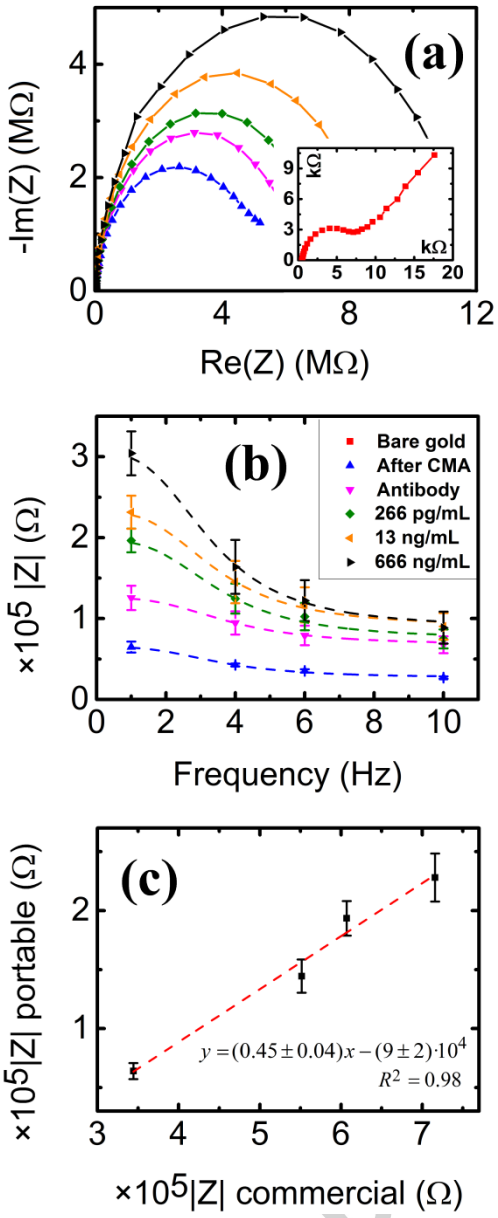

Fig. 6: (a) Nyquist (a) and Bode amplitude (b) plots showing the detection of varying TNF-α concentration measured with the commercial station and the developed potentiostat, respectively. In both cases, an increase in polarization resistance with increasing steps in the functionalization procedure, i.e. from bare gold, CMA-coated gold and anti-TNF-α antibody to cytokines interaction, can be clearly appreciated. (c) Linear calibration curve showing the relation between the absolute impedance at 1 Hz measured by the portable and the commercial potentiostats.

4. Conclusions

A low-cost and miniaturized potentiostat was designed, developed and interfaced with a miniaturized and integrated biosensor array to perform electrochemical impedance analysis at a critical frequency range. The potentiostat prototype was sized 12 × 7 × 2 cm^3, weighed 70 g and had an approximate manufacturing cost of 300 USD. The electronic board design is flexible enough to leave a door open to completely autonomous operation and to the application of several electrochemical techniques, such as amperometry, cyclic voltammetry and electrochemical impedance spectroscopy, and future steps will consider remote data

transmission through Internet connection. Impedance spectroscopy is one of the most precise techniques, and it provides detailed characterization of label-free biosensors. Our electronic device was tested on anti-TNF-α-immobilized over CMA-modified gold microelectrodes for the detection of TNF-α cytokines at several concentrations. Surface modification and antibody functionalization of gold electrodes were measured with the portable device, which also successfully discriminated between three concentrations of TNF-α cytokines. We measured impedance absolute values in the range of few hundreds kΩ, features that are comparable to those obtained with the VMP3 commercial impedance analyzer. Our approach succeeds in fixing some of which we consider important issues reported in the literature, such as the performance of measurements at low frequencies (below 10 Hz), the determination of the sensor's contribution to its complex impedance and the performance of eight parallel measurements for multiplexed analyte detection or for single measurement redundancy. The results suggest that the developed device could be useful and easily embeddable in POC environments.

Acknowledgements

The research leading to these results has received funding from the European Union's 7FP (*SEA-on-a-CHIP*, Grant Agreement no. 614168) and the European Union's Horizon 2020 (HEARTEN, Grant Agreement no. 643694). R.P. acknowledges an FPU grant from the Spanish Ministerio de Educación, Cultura y Deporte.

References

Adachi, M., Sakamoto, M., Jiu, J., Ogata, Y., Isoda, S., 2006. J. Phys. Chem. B 110, 13872–13880.

Ahmadi, M.M., Jullien, G., Iniewski, K., 2008. VLSI Circuits Biomed. Appl. 309–326.

Ahmadi, M.M., Jullien, G., others, 2009. Circuits Syst. I Regul. Pap. IEEE Trans. 56, 1339–1348.

Alcacer, A., Streklas, A., Baraket, A., Zine, N., Errachid, A., Bausells, J., 2017. SPIE Microtechnologies. p. 102460H - 102460H.

Ametek Process & Analytical (Newark, DE, USA), 2015. Parstat MC-1000 [WWW Document]. URL http://www.ameteksi.com/products/potentiostats/multichannel/parstat-mc (accessed 9.11.17).

Baraket, A., Lee, M., Zine, N., Besseuille, F., Yaakoubi, N., Trivella, M.G., Bausells, J., Zabala, M., Jaffrezic-Renault, N., Errachid, A., 2011. Int J Artif Organs 34, 661.

Baraket, A., Lee, M., Zine, N., Sigaud, M., Bausells, J., Errachid, A., 2016a. Biosens. Bioelectron. 93, 170-175.

Baraket, A., Lee, M., Zine, N., Yaakoubi, N., Bausells, J., Errachid, A., 2016b. Microchim. Acta 183, 2155–2162.

Barzen, C., Brecht, A., Gauglitz, G., 2002. Biosens. Bioelectron. 17, 289–295.

Bellagambi, F.G., Baraket, A., Longo, A., Vatteroni, M., Zine, N., Bausells, J., Fuoco, R., Di

Francesco, F., Salvo, P., Karanasiou, G.S., Fotiadis, D.I., 2017. Sensors Actuators B Chem. 251, 1026-1033.

Benlarbi, M., Blum, L.J., Marquette, C.A., 2012. Biosens. Bioelectron. 38, 220–225.

Bhat, A., 2012. Stabilize your transimpedance amplifier. Appl. Note 5129.

Bio-Logic Science Instruments (Seyssinet-Pariset, France), 2016. VMP3 [WWW Document]. URL http://www.bio-logic.net/en/products/potentiostat-galvanostat-eis/vmp3-modular-16-channels-potentiostat/ (accessed 9.11.17).

Bisquert, J., Bertoluzzi, L., Mora-Sero, I., Garcia-Belmonte, G., 2014. J. Phys. Chem. C 118, 18983–18991.

Bisquert, J., Garcia-Belmonte, G., Fabregat-Santiago, F., Bueno, P.R., 1999. J. Electroanal. Chem. 475, 152–163. doi:http://dx.doi.org/10.1016/S0022-0728(99)00346-0

Boyd, M., Woolley, T., 2016. Surg. 34, 91–93.

Burdett, R., 2005. Amplitude Modulated Signals: The Lock-in Amplifier. Handb. Meas. Syst. Des.

Caruso, R., Trunfio, S., Milazzo, F., Campolo, J., De Maria, R., Colombo, T., Parolini, M., Cannata, A., Russo, C., Paino, R., Frigerio, M., Martinelli, L., Parodi, O., 2010. ASAIO J. 56, 313–318.

Caruso, R., Verde, A., Cabiati, M., Milazzo, F., Boroni, C., Del Ry, S., Parolini, M., Vittori, C., Paino, R., Martinelli, L., Giannessi, D., Frigerio, M., Parodi, O., 2012. J. Hear. Lung Transplant. 31, 625–633.

CH Instruments, Inc. (Austin, TX, USA), 2017. CHI660E [WWW Document]. URL http://www.chinstruments.com/chi600.shtml (accessed 9.11.17).

Chin, C.D., Linder, V., Sia, S.K., 2012. Lab Chip 12, 2118–2134.

Cruz, A.F.D., Norena, N., Kaushik, A., Bhansali, S., 2014. Biosens. Bioelectron. 62, 249–254.

Feldman, A.M., Combes, A., Wagner, D., Kadakomi, T., Kubota, T., Li, Y.Y., McTiernan, C., 2000. J. Am. Coll. Cardiol. 35, 537–544.

Gamry Instruments (Warminster, PA, USA), 2017. Gamry 1000E [WWW Document]. URL https://www.gamry.com/potentiostats/interface-1000e-potentiostat/ (accessed 9.11.17).

Gomaa, D., Shinn, J.O., Dowd, J.R., Branson, R.D., 2016. P. Respir. Care 61.

Gullestad, L., Ueland, T., Vinge, L.E., Finsen, A., Yndestad, A., Aukrust, P., 2012. Cardiology 122, 23–35.

Hormiangz LLC (Longmont, CO, USA), 2014. MicroAnalyzer 160C [WWW Document]. URL https://universeneeds.com/ec_100C_series.html (accessed 9.11.17).

Jessup, M., Brozena, S., 2003. N. Engl. J. Med. 348, 2007–2018.

Kaptoge, S., Seshasai, S.R.K., Gao, P., Freitag, D.F., Butterworth, A.S., Borglykke, A., Di Angelantonio, E., Gudnason, V., Rumley, A., Lowe, G., Jorgensen, T., Danesh, J., 2014. Eur. Heart J. 35, 578–589.

Kaushik, A., Vasudev, A., Arya, S.K., Pasha, S.K., Bhansali, S., 2014. Biosens. Bioelectron. 53, 499–512.

Kongsuphol, P., Ng, H.H., Pursey, J.P., Arya, S.K., Wong, C.C., Stulz, E., Park, M.K., 2014. Biosens. Bioelectron. 61, 274–279.

Lasia, A., 2002. Electrochemical impedance spectroscopy and its applications, in: Modern Aspects of Electrochemistry. Springer, pp. 143–248.

Lee, M., Zine, N., Baraket, A., Zabala, M., Campabadal, F., Caruso, R., Trivella, M.G., Jaffrezic-Renault, N., Errachid, A., 2012. Sensors Actuators B Chem. 175, 201–207.

Li, J., Macdonald, J., 2016. Biosens. Bioelectron. 83, 177–192.

Li, Z., Ye, Z., Fu, Y., Xiong, Y., Li, Y., 2016. Anal. Methods 8, 548–553.

Liu, Y., Kwa, T., Revzin, A., 2012. Biomaterials 33, 7347–7355.

Liu, Y., Zhou, Q., Revzin, A., 2013. Analyst 138, 4321–4326.

Longo, A., Baraket, A., Vatteroni, M., Zine, N., Baussells, J., Di Francesco, F., Karanasiou, G.S., Fotiadis, D.I., Menciassi, A., Errachid, A., 2016. Procedia Eng. 168, 97–100.

Maurer, M., Burri, S., de Marchi, S., Hullin, R., Martinelli, M., Mohacsi, P., Hess, O.M., 2010. Int. J. Cardiol. 141, 32–38.

Navarri, R., Lunghetti, S., Cameli, M., Mondillo, S., Favilli, R., Scarpini, F., Puccetti, L., 2015. IJC Hear. Vasc. 7, 153–157.

Nymo, S.H., Hulthe, J., Ueland, T., McMurray, J., Wikstrand, J., Askevold, E.T., Yndestad, A., Gullestad, L., Aukrust, P., 2014. Eur. J. Heart Fail. 16, 68–75.

Ooi, K.G.-J., Galatowicz, G., Towler, H.M.A., Lightman, S.L., Calder, V.L., 2006. Invest. Ophthalmol. Vis. Sci. 47, 272–277.

Petryayeva, E., Algar, W.R., 2014. Anal. Chem. 86, 3195–3202.

Pui, T.-S., Agarwal, A., Ye, F., Huang, Y., Chen, P., 2011. Biosens. Bioelectron. 26, 2746–2750.

Pui, T.S., Kongsuphol, P., Arya, S.K., Bansal, T., 2013. Sensors Actuators B Chem. 181, 494–500.

Qureshi, A., Gurbuz, Y., Niazi, J.H., 2012. Sensors Actuators B Chem. 171, 62–76.

Randles, J.E.B., 1947. Discuss. Faraday Soc. 1, 11–19.

Sánchez-Tirado, E., Salvo, C., González-Cortés, A., Yáñez-Sedeño, P., Langa, F., Pingarrón, J.M., 2017. Anal. Chim. Acta 959, 66–73.

Scofield, J.H., 1994. Am. J. Phys. 62, 129–133.

Slaughter, M.S., Pagani, F.D., Rogers, J.G., Miller, L.W., Sun, B., Russell, S.D., Starling, R.C., Chen, L., Boyle, A.J., Chillcott, S., Adamson, R.M., Blood, M.S., Camacho, M.T., Idrissi, K.A., Petty, M., Sobieski, M., Wright, S., Myers, T.J., Farrar, D.J., 2010. J. Hear. Lung Transplant. 29, S1-S39.

Soman, G., Yang, X., Jiang, H., Giardina, S., Mitra, G., 2011. J. Immunol. Methods 373, 181–191.

ter Heijne, A., Schaetzle, O., Gimenez, S., Navarro, L., Hamelers, B., Fabregat-Santiago, F., 2015. Bioelectrochemistry 106, 64–72.

Torre-Amione, G., Kapadia, S., Benedict, C., Oral, H., Young, J.B., Mann, D.L., 1996. J. Am. Coll. Cardiol. 27, 1201–1206.

Wang, J., 2006. Biosens. Bioelectron. 21, 1887–1892.

Wang, Q., Moser, J.-E., Grätzel, M., 2005. J. Phys. Chem. B 109, 14945–14953. doi:10.1021/jp052768h

Wang, Y., Wang, W., Yu, L., Tu, L., Feng, Y., Klein, T., Wang, J.-P., 2015. 70, 61–68.

Watson, C.J., Ledwidge, M.T., Phelan, D., Collier, P., Byrne, J.C., Dunn, M.J., McDonald, K.M., Baugh, J.A., 2011. Circ. Hear. Fail. 4, 188–197.

Yin, Z., Liu, Y., Jiang, L.-P., Zhu, J.-J., 2011. Biosens. Bioelectron. 26, 1890–1894.

Yu, X., Esanu, M., MacKay, S., Chen, J., Sawan, M., Wishart, D., Hiebert, W., 2016. 2016 IEEE International Symposium on. pp. 1518–1521.

ZAHNER-elektrik GmbH \& Co KG (Kronach, Germany), 2017. ZENNIUM Electrochemical Workstation [WWW Document]. URL http://zahner.de/products/external-potentiostats.html (accessed 9.11.17).

Zensor Research & Development (Taichung, Taiwan), 2016. ACIP100 [WWW Document]. URL http://www.zensor.com.tw/index_en.html (accessed 9.11.17).

Zhang, D., Lu, Y., Zhang, Q., Liu, L., Li, S., Yao, Y., Jiang, J., Liu, G.L., Liu, Q., 2016. Sensors Actuators B Chem. 222, 994–1002.

Highlights

- There is an increasing demand for miniaturized biomedical and environmental sensor systems for point-of-care (POC) applications.
- A self-contained microelectrode-based biosensor array integrated with a portable, miniaturized and parallel-screening potentiostat is presented.
- A digital post-processing stage based on a lock-in filter was implemented and an easy-to-use graphical user interface (GUI) was developed in MATLAB.
- Electrochemical impedance measurements were performed on functionalized microelectrodes for the detection of TNF-α cytokines as a proof of concept.

- There is an increasing demand for miniaturized biomedical and environmental sensor systems for point-of-care (POC) applications.
- A self-contained microelectrode-based biosensor array integrated with a portable, miniaturized and parallel-screening potentiostat is presented.
- A digital post-processing stage based on a lock-in filter was implemented and an easy-to-use graphical user interface (GUI) was developed in MATLAB.
- Electrochemical impedance measurements were performed on functionalized microelectrodes for the detection of TNF-α cytokines as a proof of concept.